NASA/TM-2001-210262

ACOUSTICAL AND FLOWFIELD CHARACTERIZATION OF A SCALED TABLETOP ROCKET

July 2001

NASA/TM-2001-210262

ACOUSTICAL AND FLOWFIELD CHARACTERIZATION OF A SCALED TABLETOP ROCKET

Max Kandula
Dynacs Inc.
John F. Kennedy Space Center, Florida

Ravi Margasahayam
Dynacs Inc.
John F. Kennedy Space Center, Florida

Michael P. Norton
Department of Mechanical and Materials Engineering
University of Western Australia
Crawley, Western Australia

Raoul E. Caimi
NASA YA-F2-T
John F. Kennedy Space Center, Florida

National Aeronautics and Space Administration
John F. Kennedy Space Center, Kennedy Space Center, Florida 32899-0001

July 2001

ABSTRACT

An analysis of the acoustical and flowfield environment for the scaled 1-pound-force (lbf) thrust tabletop motor was performed. This tabletop motor from NASA Stennis Space Center is composed of Plexiglas burning in gaseous oxygen with a graphite insert for the nozzle portion. The nozzle has a throat diameter of 0.2 inch and an exit diameter of 0.38 inch. With a chamber pressure at 55 pounds per square inch absolute (psia), a normal shock is formed immediately downstream of the nozzle exit plane as the combustion products exhaust into the ambient at atmospheric pressure. The jet characterization is based on computational fluid dynamics (CFD) in conjunction with Kirchhoff surface integral formulation and compared with correlations developed for measured rocket noise and a pressure fluctuation scaling (PFS) method. Predictions and comparisons are made for the overall sound pressure levels (OASPL's) and spectral dependence of sound pressure level (SPL). The overall objective of this effort is to develop methods for scaling the acoustic and flowfield environment of rockets with a wide range of thrust (1 lbf to 1 million lbf).

ACKNOWLEDGEMENT

The authors are greatly indebted to Dr. William St. Cyr of the Propulsion Directorate of NASA/ Stennis Space Center for providing the tabletop rocket model for testing purposes. Additionally, the authors wish to thank Robert Field of NASA/Stennis Space Center for providing data on the tabletop rocket motor and useful discussions, and Dr. Denis Karczub of SVT-Engineering Consultants in Western Australia for assistance with the pressure fluctuation scaling method. Thanks are due to Dr. Pieter Buning of NASA Langley Research Center for discussions with regard to the OVERFLOW code and to Geoffrey Rowe of Dynacs Inc. for assistance in the spectral decomposition of CFD data.

Thanks are also due to Stanley Starr, Chief Engineer, Dynacs Inc. for providing a detailed review of the manuscript. This work was performed under KSC task orders 419 and 493, with Augusto (Gus) Venegas as the Project Manager.

TABLE OF CONTENTS

Section	Title	Page
1.	INTRODUCTION	1
2.	DESCRIPTION OF THE TABLETOP ROCKET	1
2.1	Nozzle Geometry	1
2.2	Nozzle Exit Conditions	2
3.	ANALYSIS	2
3.1	CFD/Kirchhoff Analysis	2
3.1.1	Axisymmetric Grid System	2
3.1.2	CFD Solution	2
3.1.3	Acoustic Solution	3
3.2	Correlation/Analytical Method	3
3.3	Pressure Fluctuation Scaling Method	3
4.	RESULTS AND COMPARISON	5
4.1	Flowfield Results	5
4.2	Acoustical Results	5
5.	CONCLUSIONS	7
6.	REFERENCES	7

ACRONYMS, ABBREVIATIONS, AND SYMBOLS

CFD	computational fluid dynamics
CO_2	carbon dioxide
dB	decibels
FFT	Fast Fourier Transform
GO_2	gaseous oxygen
Hz	hertz
kHz	kilohertz
KSC	John F. Kennedy Space Center
LaRC	Langley Research Center
Lbf	pound force
LNG	liquified natural gas
LST	Launch Systems Testbed
NASA	National Aeronautics and Space Administration
OASPL	overall sound pressure level (ref. 20 μPa)
PFS	pressure fluctuation scaling
psia	pounds per square inch absolute
°R	degree rankine
RNP	rocket noise program
SPL	sound pressure level (ref. 20 μPa)

Nomenclature

c = sound speed, $\sqrt{\gamma g_c R_u T / W}$, ft/s

d_j = nozzle exit diameter, ft

F = total thrust, lbf

f = frequency, Hz

g_c = gravitational constant, (lbm-ft/lbf.s^2)

I = specific impulse (sec)

M = Mach number, V / c

p = static pressure, lbf/ft^2

p' = acoustic pressure disturbance, $p - p_m$, lbf/ft^2

Re = Reynolds number, $\rho u_j d_j / \mu$

R_u = universal gas constant, lbf.ft/(lbm-mole.R)

r_j = nozzle exit radius, ft

St = Strouhal number, $f d_j / u_j$

T = temperature, R

u = axial velocity, ft/s

u_c = jet center-line velocity at exit, ft/s

V = velocity, m/s
W = molecular weight, lbm/lbm-mole
x = axial distance from the nozzle exit, ft
z = radial distance from jet axis, ft

Greek Symbols

μ = dynamic viscosity, lbm.ft/s
ρ = density, lbm/ft^3
γ = isentropic exponent
Φ = fluctuating pressure spectral density, dimensionless
ω = circular frequency, radians/s
Ω = Strouhal number (pressure fluctuation method)

Subscripts

c = centerline
e = nozzle exit
j = jet
t = stagnation or total, or nozzle throat
∞ = ambient

1. INTRODUCTION

Acoustic loads in a launch vehicle environment represent a principal source of structural vibration and may be critical to the proper functioning of vehicle components, ground support structures, and equipment in the immediate vicinity of the launch pad. A knowledge of acoustic loads, including the overall sound pressure level (OASPL), sound pressure level (SPL) spectrum, and the distribution (or correlation) of surface acoustic loads is necessary to provide the input for vibroacoustic analysis and evaluation of structural integrity. In the design of launch vehicles, it is highly desirable that data on acoustic loads (near-field and far-field noise levels) be generated both analytically and from testing of small-scale and full-scale models. Since full-scale acoustic and vibration testing is often cost prohibitive, the option of small-scale testing combined with analysis methods remains as a practical alternative. Accurate characterization of acoustic loads on launch pad structures thus proves to be a formidable challenge.

At NASA Kennedy Space Center, a Launch Systems Testbed (LST) is currently under development to establish a capability to simulate small-scale launch vehicle environment for use in testing and evaluation of launch pad designs for future space vehicles. The test program provides for the scale model testing of cold jets (nitrogen), hot inert jets (helium), and combusting jets (solid/liquid rocket fuels). Concurrently, prediction methods are also under development to complement the small-scale test program. These prediction methods include computational fluid dynamics (CFD), analytical correlations, and pressure fluctuation scaling (PFS) methods.

Noise from subsonic jets is mainly due to turbulent mixing, comprising the contributions of large-scale and fine-scale structures (Lighthill, 1952, 1954). The turbulent mixing noise is mainly broadband. In perfectly expanded supersonic jets, the large-scale mixing noise manifests itself primarily as Mach wave radiation, caused by the supersonic convection of turbulent eddies with respect to the ambient fluid. In imperfectly expanded supersonic jets, additional noise is generated on account of broadband shock noise and screech tones.

This report summarizes the analytical studies of a small-scale tabletop rocket that is being acquired from NASA Stennis Space Center for the purpose of establishing the initial test facility and instrumentation. This tabletop motor has Plexiglas fuel burning in gaseous oxygen (GO_2) with an off-design nozzle (overexpanded exit Mach number of 2.6 and 1 lbf thrust). An important characteristic of the tabletop rocket is the existence of a normal shock in the immediate downstream of the nozzle exit, resulting in a subsonic jet structure. Comparisons of OASPL and SPL spectrum are presented for CFD simulations, rocket noise correlations, and the PFS method.

2. DESCRIPTION OF THE TABLETOP ROCKET

2.1 NOZZLE GEOMETRY

Figure 1 shows a schematic of the nozzle geometry for the tabletop motor, as obtained from NASA Stennis Space Center (Field 2001). Both the convergent and the divergent portions of the nozzle are conical. The nozzle has a throat diameter of 0.2 inch and an exit diameter of 0.38 inch. The locations of three points A, E, and X for comparisons are indicated here.

2.2 NOZZLE EXIT CONDITIONS

Representative data on combustion chamber conditions and gas compositions were also obtained from Field (2001). The combustion gas is approximated as carbon dioxide (CO_2). Initial isentropic calculations, ignoring boundary layer effects, showed that a normal shock would be formed downstream of the nozzle exit. The nozzle exit conditions as derived from isentropic expansion in the nozzle are shown in table 1.

3. ANALYSIS

3.1 CFD/KIRCHHOFF ANALYSIS

The CFD/Kirchhoff analysis is based on the application of a CFD code for identifying the noise sources in the source-field and Kirchhoff surface integral for the propagation of sound radiation to the near-field and the far-field. In particular, the OVERFLOW CFD code (Buning et al., 2001) of NASA Langley Research Center (LaRC) is used for computing the instantaneous flowfield. This code solves the three-dimensional compressible turbulent flow Navier-Stokes equations in generalized coordinates. A one-equation turbulence model of Spalart-Allmaras (1992) is considered. The OVERFLOW code, in its present form, is designed primarily for the prediction of steady or unsteady turbulent flowfield and is used widely to model aerodynamic flows. It does not however provide the necessary time-dependent boundary conditions for handling the reflection-free acoustic propagation. Therefore appropriate modifications to the code were made to provide a set of time-dependent reflection-free boundary conditions (includes periodic inflow, outflow, and radiation).

For the acoustic radiation, the Kirchhoff code YORICK developed by Pilon and Lyrintzis (1998) of Purdue University was considered. The Kirchhoff surface, enclosing the nonlinear source region, is chosen in a region where the linear wave equation is valid. The Kirchhoff method does not suffer dissipation and dispersion errors that could be encountered when the near-field and far-field sounds are directly calculated with the CFD code. By restricting the use of CFD methods to the near-field region for source identification, computational requirements are greatly reduced.

3.1.1 AXISYMMETRIC GRID SYSTEM. For the CFD computations, an axisymmetric grid of 200x100 (200 grid points in the axial direction and 100 grid points in the radial direction) is considered. Figure 2 shows a schematic of the computational grid. A grid length of 60 jet radii and a grid radius of 10 radii are considered. The grid is clustered in the axial direction near the nozzle exit for handling shocks and other high gradients in the flow and also near the outer radius of the nozzle for resolving shear layers.

3.1.2 CFD SOLUTION. Appropriate time-dependent boundary conditions were applied to ensure reflection-free boundaries. An outflow boundary condition of Thompson type (Thompson 1990) is applied at the outflow boundary, which maintains the mean static pressure at the ambient value. An acoustic radiation boundary condition of Tam and Webb (1993) is applied at the lateral boundary. At the inlet, the flow variables are specified based on the nozzle exit conditions. The CFD solution converged after about 15,000 time-step iterations (the code is run in a

time-accurate manner) before a periodic state is established. The solution is obtained on an IRIX workstation (SGI Indigo machine). About 30 hours of computing time are required for the solution to achieve a periodic state.

3.1.3 ACOUSTIC SOLUTION. After a periodic state is established, the appropriate data from CFD is communicated to the Kirchhoff code. The Kirchhoff surface is a cylindrical surface coinciding with a grid line. The radius of the Kirchhoff surface is taken as about 6 radii from the jet axis. Only the lateral surface of the cylinder is taken into account ignoring cylinder ends due to the effects of nonlinearities. Specifically, the data to be specified on the Kirchhoff surface include the instantaneous pressure, the pressure-time derivative, and the pressure gradient normal to the surface. The Kirchhoff code then computes the pressure-time signals and the OASPL in the near- and the far-field. From the pressure-time signals, it is possible to compute the SPL spectrum at any location with the aid of Fast Fourier Transform (FFT). Inside the Kirchhoff surface, the OASPL and the SPL spectrums are computed directly from the CFD solution for the instantaneous pressure. A more detailed account of the CFD and the Kirchhoff methods is provided in a report by Kandula and Caimi (2001).

3.2 CORRELATION/ANALYTICAL METHOD

Leneman (1973) proposed an empirical correlation for the OASPL as

$$\text{OASPL (dB)} = 115 + 10\ \log(\text{FI}) - 20\log(x) \tag{1a}$$

where F denotes the total thrust (lbf), I the specific impulse (sec), and x the axial distance (ft) in the far-field from the jet exit plane. Margasahayam and Caimi (1999 and 2000) developed an analytical model to predict the far-field noise generated by rockets in the holddown state, representative of static tests. The OASPL is expressed by an extension of Leneman equation as

$$\text{OASPL (dB)} = 115 + 10\log(\text{FI}) - 20\log(x) - 20\,x\,10^{(-x/50)} \tag{1b}$$

The fourth term on the right-hand side is the near-field correction term due to Margasahayam and Caimi (1999). This equation represents a first-order estimate only and does not account for the effects of spectral composition, directivity, etc.

The NASA SP-8072 method (1971) is considered in the rocket noise program (RNP) of Margasahayam and Caimi (1999), which represents a more accurate correlation compared to the Leneman correlation. It computes OASPL and SPL spectrums by an empirical correlation based on the normalized relative power spectrum as a function of Strouhal number derived from a number of solid- and liquid- fueled chemical rockets.

3.3 PRESSURE FLUCTUATION SCALING METHOD

The method of pressure fluctuation scaling due to Norton et al. (1999), which has been successfully used for industrial gas piping networks, industrial gas turbine exhausts, blowdown systems

in liquefied natural gas (LNG) plants, and offshore platforms, etc., is discussed in the following paragraphs.

The fluctuating pressure spectrum at the nozzle exit (after the shock wave) is estimated via a pressure fluctuation scaling technique based on (1) laboratory data for a turbulent wall pressure spectrum in a cylindrical shell, (2) a turbulent wall pressure spectrum on a flat plate, and (3) a fluctuating wall pressure spectrum downstream of a severe internal flow disturbance such as a depressurization valve or a 90-degree mitre bend and using the post-shock centerline input data (static pressure, static temperature, density, flow velocity, and Mach number) from the CFD results. The nondimensional fluctuating pressure spectral density Φ_p is given by

$$\Phi_p(\Omega) = \frac{4G_p(\omega)}{\rho^2 U^3 a} \tag{2a}$$

where the nondimensional frequency Ω (Strouhal number)

$$\Omega = \omega a / U \tag{2b}$$

where G_p is the fluctuating pressure spectral density, ρ the gas density, U the flow velocity, a the nozzle exit radius, and $\omega = 2\pi f$. Controlled laboratory measurements of G_p, ρ, and U for a given turbulent boundary layer flow in a shell of internal radius a are used to calculate the nondimensional fluctuating pressure spectrum Φ_p according to equation (2a). The frequency axis is simultaneously scaled according to equation (2b). Hence, a spectrum of nondimensional fluctuating turbulent pressure spectral density Φ_p against nondimensional frequency Ω is obtained. The turbulent wall pressure spectrum (shell or flat plate) provides a lower level, and the severe internal flow disturbance provides the upper level for scaling purposes.

The sound spectrum is then calculated at the exit downstream of the shock. Power spectral estimates of fluctuating pressure against radian frequency for the tabletop rocket are obtained from

$$S_p(\omega_i) = \frac{\Phi_p(\Omega)\rho^2 U^3 a \Delta\omega_i}{4} \tag{3a}$$

where

$$\omega_i = U\Omega_i / a \tag{3b}$$

and $\Delta\omega_i$ is the nominal bandwidth of band i with center frequency ω_i.

Correction factors are then applied for the open jet exhausting out of the nozzle. At this stage, a 1/r decay with distance from the nozzle is assumed for circumferential radiation away from the exit plane (e.g., position A, figure 1). The 1/r decay is also considered for post shock centerline decay (e.g., position X) because the mean flow will enhance/convect the monopole- and dipole-type radiation from the duct exit. These assumptions need to be refined but serve as an order of magnitude prediction at the present time.

The results were computed in linear octave frequency bands and in spectral values [decibel (dB) linear/hertz (Hz)]. Both the lower- and the upper-limit scaling spectra were utilized to estimate the pressure fluctuations downstream of the shock wave at all three locations downstream of the nozzle exit. The pressure fluctuation scaling results presented here thus provide both lower- and upper-level estimates at locations A, E, and X for completeness.

4. RESULTS AND COMPARISON

4.1 FLOWFIELD RESULTS

The axial velocity contours and the temperature contours from CFD are displayed in figures 3 and 4 respectively. An overview of the jet flowfield structure, including the shear layer mixing, is evident from these plots. A normal shock is formed near the exit plane, thus resulting in a subsonic flow downstream of the exit. The existence of a normal shock outside the nozzle is to be expected based on the isentropic expansion/normal-shock calculations for the nozzle with the given area ratio (Mach number) and chamber to ambient pressure ratio (Shapiro 1953). The temperature contours suggest the formation of vortical structures in the shear layer.

Figures 5 through 8 represent the centerline variation of important flow parameters (static pressure, static temperature, flow velocity, and Mach number). Figure 5 displays typical static pressure excursions in the core region and the pressure approaches the ambient value far downstream of the nozzle exit plane. It is inferred from figure 7 for the centerline axial velocity distribution that the core length of the jet extends to about 25 jet radii from the exit plane. As evident from figure 8, the average Mach number in the core region downstream of the shock is about 0.6, characterizing the jet as subsonic.

4.2 ACOUSTICAL RESULTS

Figure 9 presents the OASPL contours in the near- and the far-field (x/r_j from –60 to 60, and z/r_j from 10 to 70) as computed by the CFD/Kirchhoff formulation. The OASPL ranges from 80 to 130 dB in this region. Two primary lobes are recognized and located downstream of the exit plane. The absence of a dominant Mach wave radiation is due to the subsonic nature of the jet. The OASPL contours within the jet, characterizing primarily the nonlinear source-field, displayed in figure 10, are evaluated directly from the CFD solution. Inside the jet shear layer, the sound pressure levels are high (as much as 180 dB), with the highest OASPL occurring about 7 jet radii downstream of the exit. The relatively high-sound levels at this position are attributable to the high-turbulence intensities in the shear layer. Figure 11 displays the OASPL distribution along the line BC, 24.52 radii from the jet axis (figure 1), as computed from CFD. The OASPL is seen to be highest near the exit plane and decreases away from the exit.

In the following plots, comparisons are made for the OASPL and spectral distribution of SPL at three representative positions A, E, and X (see figure 1). Point A (x/r_j=0, and z/r_j=24.5) is located in the exit plane, 24.5 jet radii away from the jet axis; point E (x/r_j=0.63, and z/r_j=0)

is situated on the jet axis, 0.63 jet radii downstream of the exit plane; and point X (x/r_j=23.5, and z/r_j=1) is stationed 23.5 jet radii downstream of the exit plane, and one jet radius away from the axis. Table 2 summarizes the comparison of OASPL at stations A, E, and X as estimated by the different methods.

The spectral composition of 1/3 octave SPL at point A in the exit plane is presented in figure 12. A similarity is noted in the SPL spectrum from the CFD and the upper-level PFS, although the SPL from the upper-level PFS exceeds the CFD result. However, both the CFD and the upper-level PFS method suggest a peak frequency of about 20 kilohertz (kHz). This peak frequency corresponds to a Strouhal number St=0.20. The lower-level PFS method produces SPL that is close to that of the CFD but produces a peak frequency of about 100 kHz, which appears somewhat overestimated. The deviation in the SPL between the upper-level and the lower-level PFS is attributable to the fact that the lower-level result is based on turbulent pressure spectrum for shell/flat plate, whereas the upper-level result is based on the pressure spectrum scaling corresponding to severe internal flow disturbance, as indicated before. High value for the peak frequency level (of the order of kHz) for the SPL distribution is a characteristic of the small-scale nozzle considered here, as to be expected from the similarity scaling provided by the Strouhal number.

A comparison of the 1/3 octave SPL content at location E on the axis downstream of the exit plane is portrayed in figure 13. In general the SPL values at E are considerably higher than those at position A, due to the near-field location of E and the effect of directivity (E is located in the jet and is also closer to the exit plane, whereas A is located in the exit plane and oriented at 90 degrees to the jet axis). A peak frequency of about 35 kHz (corresponding to St=0.35) is indicated by CFD, the NASA-SP method, and the PFS upper-level method. The CFD results for the SPL are higher than those from the NASA-SP method. In the case of the PFS method, the upper-level values for the SPL are closer to the CFD, whereas the lower-level results match well with the NASA-SP method.

Figure 14 compares the spectral distribution of 1/3 octave SPL at location X, which is downstream of location E but one jet radius away from the axis. In general the sound pressure levels at X are smaller than those at E. A reduced peak frequency of about 25 kHz (corresponding to St=0.25), relative to location E, is indicated by CFD, the NASA-SP method, and the PFS upper-level method. The SPL variation between the various methods at position X is somewhat smaller as compared to that at positions A and E.

A comparison of the 1/3 octave SPL at locations A, E, and X as predicted by CFD is shown in figure 15. Downstream of the exit plane, the peak frequency level is increased in the near-field, as the distance from the exit plane is decreased. While there appears to be a similarity in the shape of the SPL spectrum between E and X, there is a departure in similarity at position A for frequencies in excess of about 40 kHz, where a rapid decline in SPL is observed. This lack of similarity in the SPL spectrum at position A is perhaps attributable to the existence of a normal shock near the nozzle exit or to the far-field directivity effects.

5. CONCLUSIONS

The CFD/Kirchhoff method provided flowfield structure and distributions of the OASPL and SPL spectrum for the tabletop rocket. As a result of the overexpansion in the nozzle, a normal shock forms in the immediate downstream of the nozzle exit, providing a subsonic jet. Vortical structures in the jet shear layer are observed. High values of OASPL (140 to 180 dB) are noted in the shear layer region comprising about 15 jet diameters downstream of the exit plane. Lower levels of OASPL (80 to 130 dB) are computed in the near- and the far-field region. Because of the very small size of the nozzle exit diameter, the jet is distinguished by high peak frequency levels (20 to 35 kHz) for the SPL spectrum.

A comparison of the results from CFD, the NASA-SP method, and the PFS method at three spatial locations (A, E, and X) showed that a similarity in shape is generally noted for the SPL composition. There is some disagreement between the different methods for the peak frequencies and the SPL values. In the jet region (positions E and X), the CFD predictions for the SPL are found to be higher than those from the NASA-SP method. The upper-level results in this region agree better with the CFD results, whereas the lower-level results match better with the NASA-SP values. In the far-field region (location A), the lower-level PFS compares better with the CFD results, while the upper-level PFS values considerably exceed the CFD predictions. A more realistic assessment of these methods can only be carried out with the aid of an experimental test program currently under development.

6. REFERENCES

Anonymous, Acoustic Loads Generated by the Propulsion System, NASA-SP-8072, June 1971.

Buning, P.G.; Jesperson D.C.; Pulliam, T.H.; Chan, W.M.; Slotnick, J.P.; Krist, S.E.; and Renze, K.J.; OVERFLOW User's manual- version 1.8, NASA Langley Research Center, February 1998.

Field, R., NASA Stennis Space Center, Personal Communication, February 2001.

Kandula, M. and Caimi, R., Simulation of Supersonic Jet Noise With the Application of OVERFLOW CFD Code and Kirchhoff Surface Integral, KSC-YA-5556, 2001.

Kirchhoff, G.R., Zur Theorie der Lichtstrahlen, Annalen der Physik und Chermie, Vol. 18, pp. 663-695, 1883.

Leneman, G., Determination of Maximum Ground Noise During a Rocket Launch- Discussion and Simple Prediction Method, Proceeding of the Institute of Environmental Sciences, April 2-5, 1973.

Lighthill, M.J., On Sound Generated Aerodynamically: I. General Theory, Proc. Roy. Soc. (London), Ser. A, Vol. 211, No. 1107, pp. 564-587, March 1952.

Lighthill, M.J., On Sound Generated Aerodynamically: II. Turbulence as a Source of Sound, Proc. Roy. Soc. (London), Ser. A, Vol. 222, No. 1148, pp. 1-32, Feb. 1954.

Margasahayam, R. and Caimi, R., Rocket Noise Prediction Program, Sixth International Congress on Sound and Vibration, Lingby, Denmark, July 1999.

Margasahayam, R. and Caimi, R., Rocket Noise Prediction Program – Application, Seventh International Congress on Sound and Vibration, Garmisch-Partenkirchen, Germany, July 2000.

Norton, M.P., Fundamentals of Noise and Vibration Analysis, Cambridge University Press, 1989.

Pilon, A.R. and Lyrintzis, A.S., Development of an Improved Kirchhoff Method for Jet Aeroacoustics, AIAA J., pp. 783-790, May 1998.

Shapiro, A.H., The Dynamics and Thermodynamics of Compressible Fluid Flow, Vol. 1, John Wiley & Sons, New York, 1953.

Spalart, P.R. and Allmaras, S.R., A One-Equation Turbulence Model for Aerodynamic Flows, AIAA-92-0439, 1992.

Tam, C.K.W. and Webb, J.C., Dispersion-Relation-Preserving Finite Difference Schemes for Computational Aeroacoustics, Journal of Computational Physics, Vol. 107, pp. 262-281, 1993.

Thompson, K.W., Time-Dependent Boundary Conditions for Hyperbolic Systems II, Journal of Computational Physics, Vol. 89, pp. 439-461, 1990.

Table 1. Summary of Nozzle Parameters

Parameter	Value
Stagnation pressure, psia	54.7
Stagnation temperature, °R	1960
Nozzle mass flow rate, lbm/s	0.0247
Nozzle throat diameter, inch	0.2
Nozzle exit diameter, inch	0.38
Exit pressure, psia	2.38
Exit temperature, °R	987
Exit velocity, ft/s	3,170
Acoustic velocity at exit, ft/s	1,195
Nozzle exit Mach number	2.65
Nozzle exit density, lbm/ft^3	0.0099
Molecular weight for CO_2	44
Specific heat ratio for CO_2	1.28
Jet exit Reynolds number	2.9×10^4
Ambient pressure, psia	14.7
Ambient temperature, °R	519

Table 2. Comparison of OASPL at Locations A, E, and X

Location	CFD	Leneman		NASA-SP-8072	PFS	
		Original	Modified		Upper Level	Lower Level
A	118	-*	-	-	153	119
E	151	175	155	125	176	130
X	140	144	124	117**	135	122

* Not applicable

** Value corresponding to $z = 0$

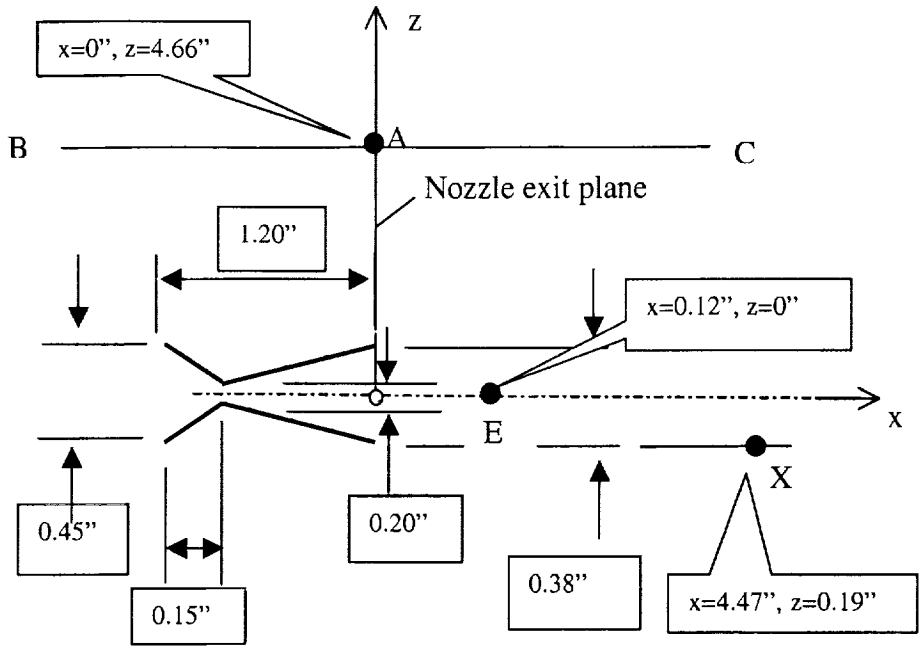

Figure 1. Schematic of the Tabletop Rocket Nozzle

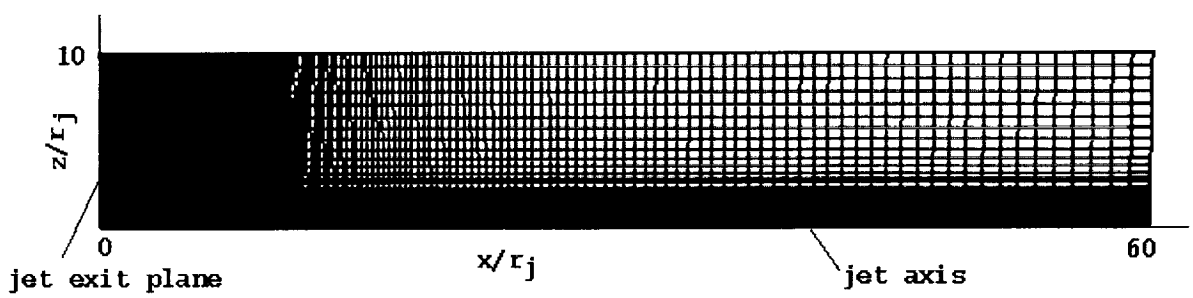

Figure 2. Axisymmetric Grid (200x100) for CFD

Figure 3. Mean Axial Velocity Contours in the Jet From CFD Solution

Figure 4. Mean Temperature Contours in the Jet From CFD Solution

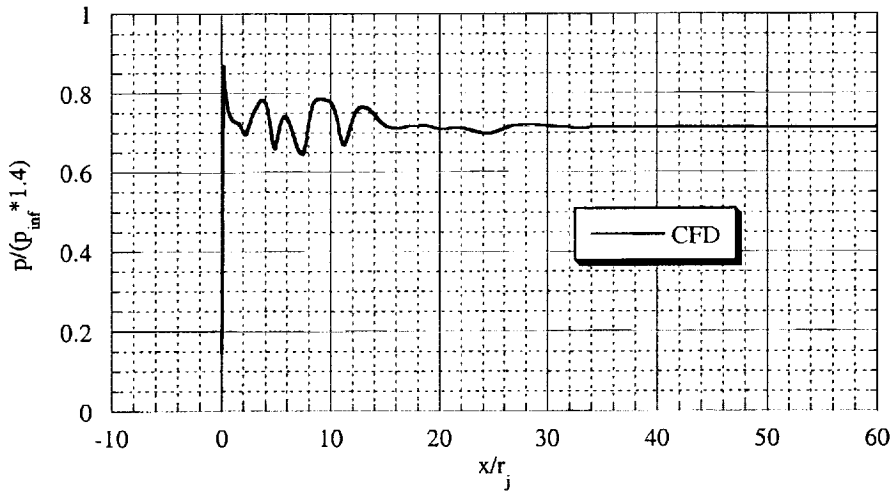

Figure 5. Jet Centerline Variation of Static Pressure From CFD

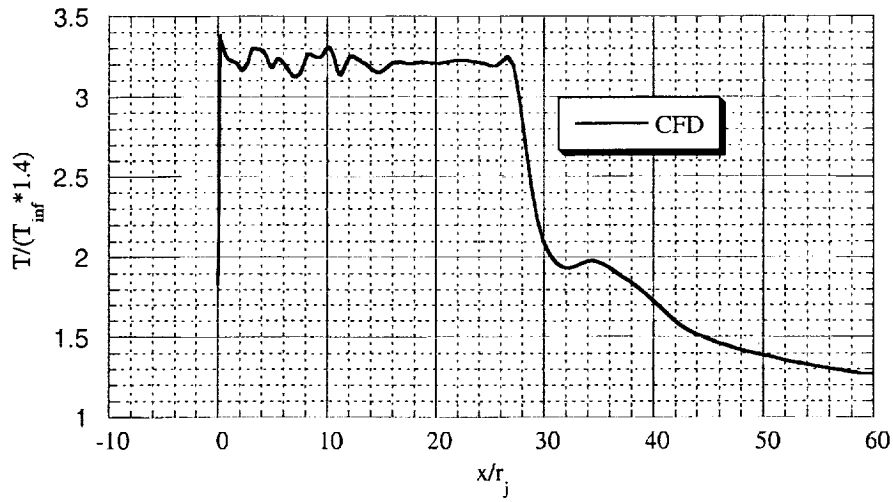

Figure 6. Jet Centerline Variation of Static Temperature From CFD

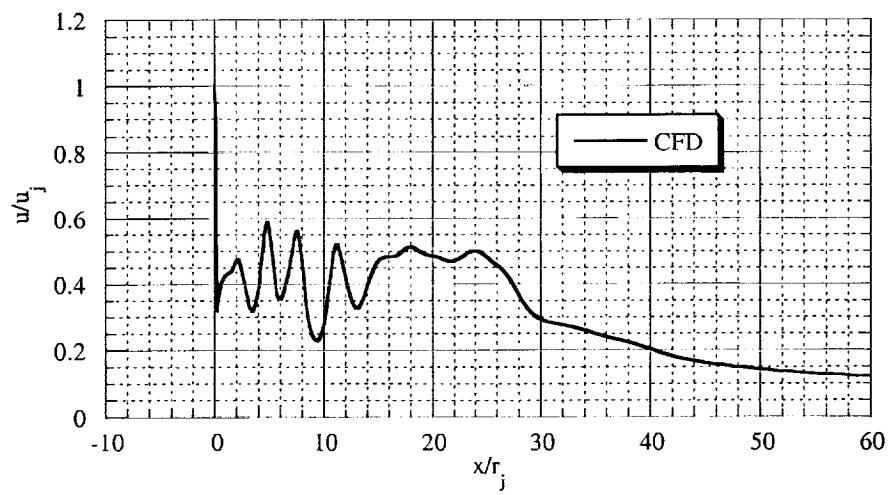

Figure 7. Jet Centerline Variation of Axial Velocity From CFD

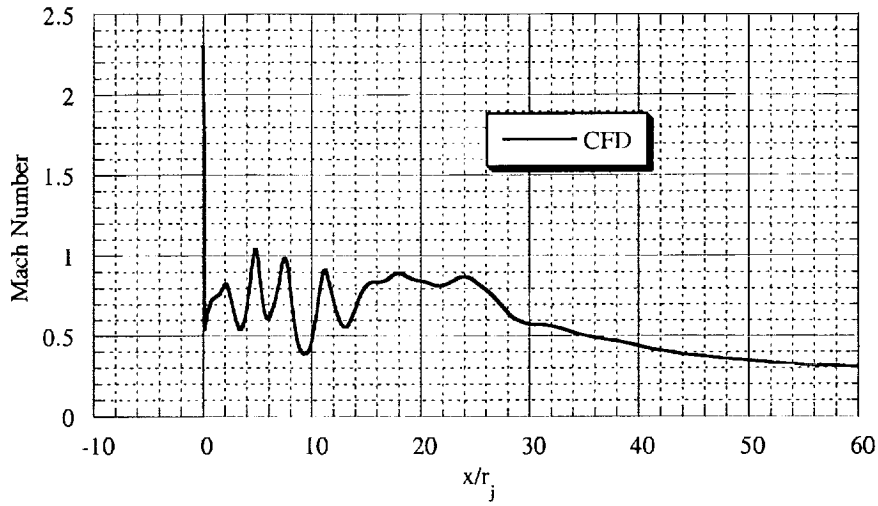

Figure 8. Jet Centerline Variation of Mach Number From CFD

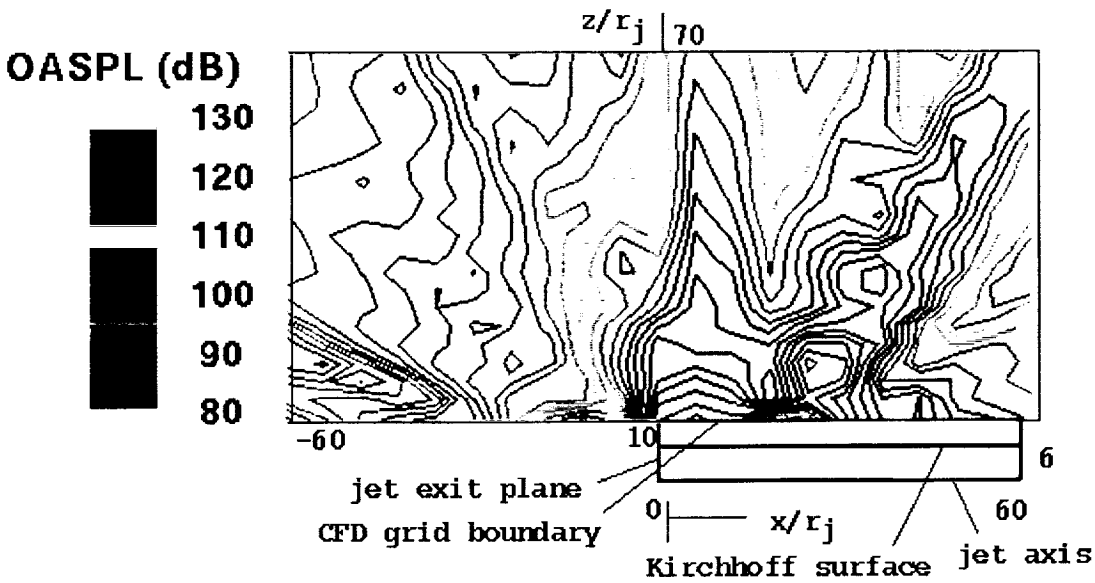

Figure 9. Contours of OASPL Predicted From CFD/Kirchhoff Method

Figure 10. Contours of OASPL in the Source-Field as Computed Directly From CFD

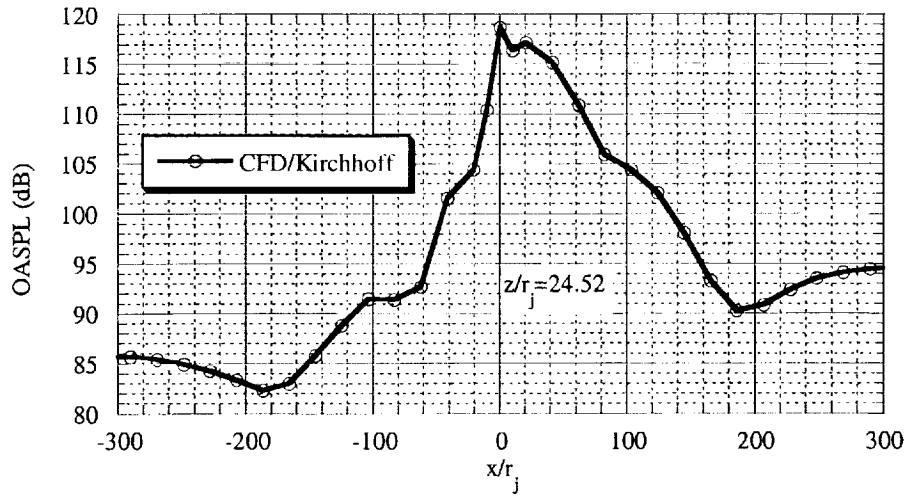

Figure 11. Axial OASPL Distribution at z/r_j=24.52 From CFD

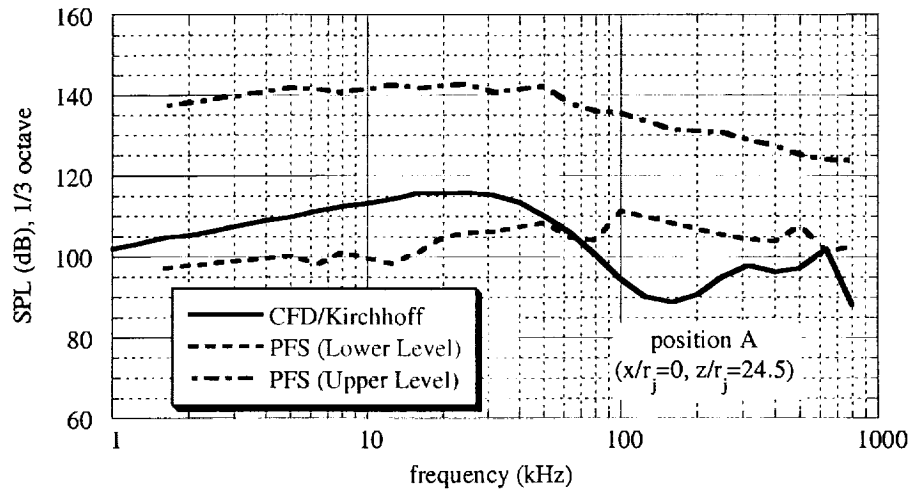

Figure 12. Comparison of 1/3 Octave Spectra at Location A.

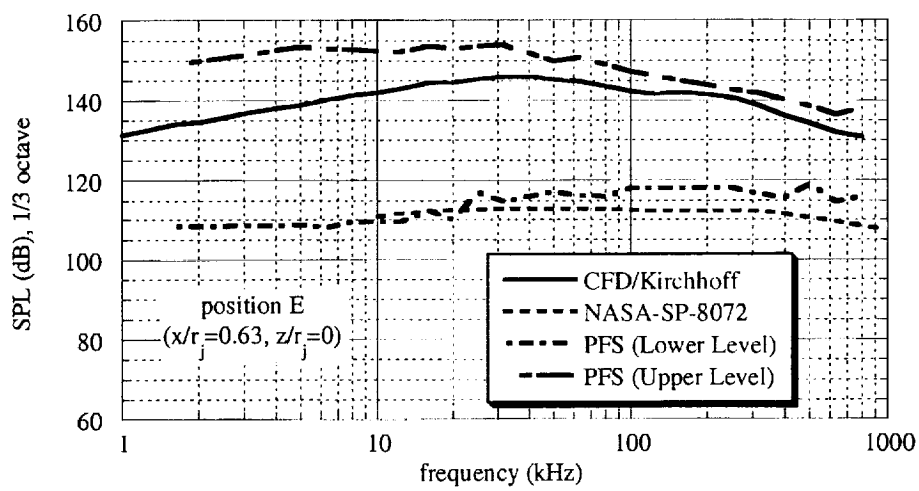

Figure 13. Comparison of 1/3 Octave SPL Spectra at Location E

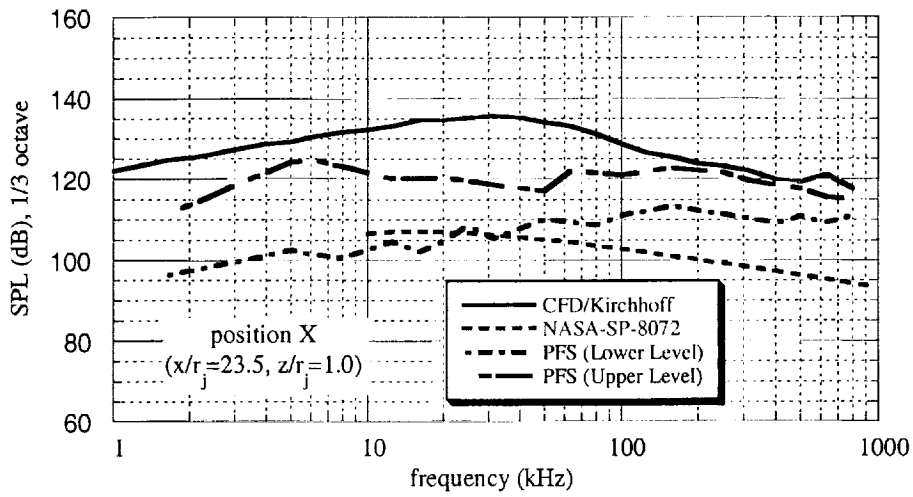

Figure 14. Comparison of 1/3 Octave SPL Spectra at Location X

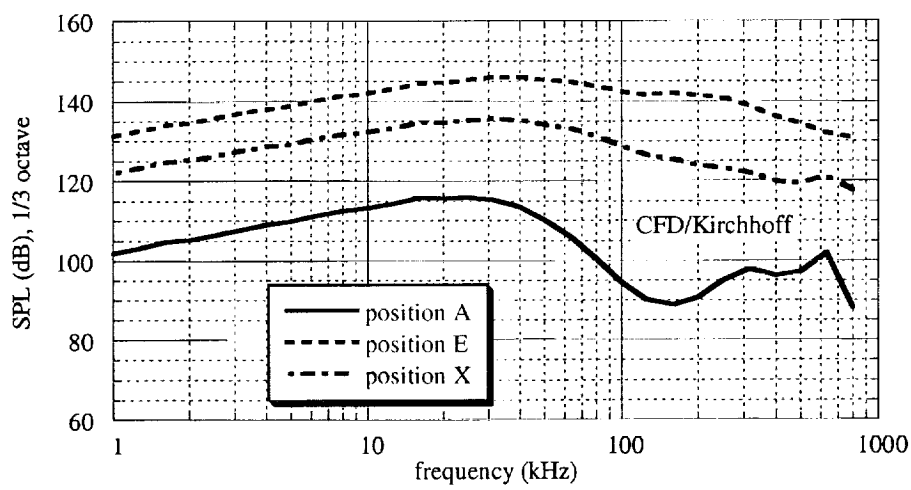

Figure 15. Comparison of 1/3 Octave SPL Spectra From CFD at A, E, and X

REPORT DOCUMENTATION PAGE

Form Approved
OMB No. 0704-0188

Public reporting burden for this collection of information is estimated to average 1 hour per response, including the time for reviewing instructions, searching existing data sources, gathering and maintaining the data needed, and completing and reviewing the collection of information. Send comments regarding this burden estimate or any other aspect of this collection of information, including suggestions for reducing this burden, to Washington Headquarters Services, Directorate for Information Operations and Reports, 1215 Jefferson Davis Highway, Suite 1204, Arlington, VA 22202-4302, and to the Office of Management and Budget, Paperwork Reduction Project (0704-0188), Washington, DC 20503.

1. AGENCY USE ONLY *(Leave blank)*	2. REPORT DATE	3. REPORT TYPE AND DATES COVERED
	July 2001	Technical Memorandum - 2001

4. TITLE AND SUBTITLE

Acoustical and Flowfield Characterization of a Scaled Tabletop Rocket

5. FUNDING NUMBERS

6. AUTHOR(S)

Max Kandula and Ravi Margasahayam, Dynacs Inc., Kennedy Space Center, FL
Michael Norton, University of Western Australia
Raoul Caimi, NASA, Kennedy Space Center, FL

7. PERFORMING ORGANIZATION NAME(S) AND ADDRESS(ES)

NASA John F. Kennedy Space Center
Kennedy Space Center, Florida 32899

8. PERFORMING ORGANIZATION REPORT NUMBER

9. SPONSORING/MONITORING AGENCY NAME(S) AND ADDRESS(ES)

National Aeronautics and Space Administration
Washington, D.C. 20546

10. SPONSORING/MONITORING AGENCY REPORT NUMBER

NASA/TM-2001-210262

11. SUPPLEMENTARY NOTES

Responsible Individual: Raoul Caimi, YA-F2-T, (321) 867-4655

12a. DISTRIBUTION/AVAILABILITY STATEMENT

Unclassified - Unlimited
Subject Category:

12b. DISTRIBUTION CODE

13. ABSTRACT *(Maximum 200 words)*

An analysis of the acoustical and flowfield environment for the scaled 1-pound-force (lbf) thrust tabletop motor was performed. This tabletop motor from NASA Stennis Space Center is composed of Plexiglas burning in gaseous oxygen with a graphite insert for the nozzle portion. The nozzle has a throat diameter of 0.2 inch and an exit diameter of 0.38 inch. With a chamber pressure at 55 pounds per square inch absolute (psia), a normal shock is formed immediately downstream of the nozzle exit plane as the combustion products exhaust into the ambient at atmospheric pressure. The jet characterization is based on computational fluid dynamics (CFD) in conjunction with Kirchhoff surface integral formulation and compared with correlations developed for measured rocket noise and a pressure fluctuation scaling (PFS) method. Predictions and comparisons are made for the overall sound pressure levels (OASPL's) and spectral dependence of sound pressure level (SPL). The overall objective of this effort is to develop methods for scaling the acoustic and flowfield environment of rockets with a wide range of thrust (1 lbf to 1 million lbf).

14. SUBJECT TERMS

Acoustical and flowfield environment, scaled tabletop rocket, thrust

15. NUMBER OF PAGES

16. PRICE CODE

17. SECURITY CLASSIFICATION OF REPORT	18. SECURITY CLASSIFICATION OF THIS PAGE	19. SECURITY CLASSIFICATION OF ABSTRACT	20. LIMITATION OF ABSTRACT
Unclassified	Unclassified	Unclassified	